

UC Berkeley

UC Berkeley Previously Published Works

Title

Radial variation in biochemical composition of the bovine caudal intervertebral disc

Permalink

<https://escholarship.org/uc/item/8zp4h390>

Journal

JOR Spine, 2(3)

ISSN

2572-1143

Authors

Bezci, Semih E
Werbner, Benjamin
Zhou, Minhao
et al.

Publication Date

2019-09-01


DOI

10.1002/jsp2.1065

Peer reviewed

RESEARCH ARTICLE

Radial variation in biochemical composition of the bovine caudal intervertebral disc

Semih E. Bezci¹  | Benjamin Werbner¹ | Minhao Zhou¹ | Katerina G. Malollari¹ | Gabriel Dorlhiac² | Carlo Carraro³ | Aaron Streets^{2,4,5} | Grace D. O'Connell^{1,6}

¹Department of Mechanical Engineering, University of California, Berkeley, California

²Berkeley Biophysics Program, University of California, Berkeley, California

³Department of Chemical and Biomolecular Engineering, University of California, Berkeley, California

⁴Department of Bioengineering, University of California, Berkeley, California

⁵Chan-Zuckerberg Biohub, San Francisco, California

⁶Department of Orthopaedic Surgery, University of California, San Francisco, California

Correspondence

Grace D. O'Connell, Department of Mechanical Engineering, University of California, 5122 Etcheverry Hall, #1740, Berkeley, CA 94720.

Email: g.oconnell@berkeley.edu

Funding information

National Science Foundation, Grant/Award Number: 1751212

Abstract

Bovine caudal discs have been widely used in spine research due to their increased availability, large size, and mechanical and biochemical properties that are comparable to healthy human discs. However, despite their extensive use, the radial variations in bovine disc composition have not yet been rigorously quantified with high spatial resolution. Previous studies were limited to qualitative analyses or provided limited spatial resolution in biochemical properties. Thus, the main objective of this study was to provide quantitative measurements of biochemical composition with higher spatial resolution than previous studies that employed traditional biochemical techniques. Specifically, traditional biochemical analyses were used to measure water, sulfated glycosaminoglycan, collagen, and DNA contents. Gravimetric water content was compared to data obtained through Raman spectroscopy and differential scanning calorimetry. Additionally, spatial distribution of lipids in the disc's collagen network was visualized and quantified, for the first time, using multi-modal second harmonic generation (SHG) and Coherent anti-Stokes Raman (CARS) microscopy. Some heterogeneity was observed in the nucleus pulposus, where the water content and water-to-protein ratio of the inner nucleus were greater than the outer nucleus. In contrast, the bovine annulus fibrosus exhibited a more heterogeneous distribution of biochemical properties. Comparable results between orthohydroxyproline assay and SHG imaging highlight the potential benefit of using SHG microscopy as a less destructive method for measuring collagen content, particularly when relative changes are of interest. CARS images showed that lipid deposits were distributed equally throughout the disc and appeared either as individual droplets or as clusters of small droplets. In conclusion, this study provided a more comprehensive assessment of spatial variations in biochemical composition of the bovine caudal disc.

KEYWORDS

animal models, biochemistry, Coherent anti-Stokes Raman, differential scanning calorimetry, intervertebral disc, Raman spectroscopy, second harmonic generation

This is an open access article under the terms of the Creative Commons Attribution-NonCommercial License, which permits use, distribution and reproduction in any medium, provided the original work is properly cited and is not used for commercial purposes.

© 2019 The Authors. JOR Spine published by Wiley Periodicals, Inc. on behalf of Orthopaedic Research Society

1 | INTRODUCTION

Animal discs have been widely adapted to study relationships between intervertebral disc structure and function. In particular, bovine caudal discs have been excellent models for studying biomechanical behavior of healthy discs, because of increased tissue availability and larger disc size.¹ Despite some morphological differences, such as increased circularity, bovine discs exhibit biochemical and mechanical properties similar to healthy human discs.^{2–6} Biochemically, bovine discs have similar water, proteoglycan, and collagen contents as young, healthy human discs.⁵ Mechanically, compressive and torsional properties of bovine caudal discs are comparable to human discs after accounting for differences in disc geometry.^{2–4,6} Moreover, the quantity of notochordal cells in human and bovine discs declines rapidly with age, an observation not seen in smaller animals (eg, rat, pig, cat, and rabbit).⁷

Various analytical techniques have been used to characterize biological tissue structure and composition. Traditional techniques include spectrophotometric assays of tissue digests and immunohistochemical staining of fixed tissues.^{8–12} More recently, alternative imaging and spectroscopy techniques have garnered significant interest, due to less destructive protocols.^{13,14} Such techniques include nonlinear optical imaging, such as Coherent anti-Stokes Raman spectroscopy (CARS) and second-harmonic generation (SHG) imaging.^{15,16} The combined use of CARS and SHG provides simultaneous, high-resolution images of collagen fibers and lipids.¹⁷ However, each measurement method has its own advantages and limitations; as such, a rigorous compositional analysis should apply a variety of analytical techniques.

It has long been known that biochemical and mechanical properties vary greatly throughout the human intervertebral disc.^{18–21} However, comparisons are largely drawn between the nucleus pulposus (NP) and the annulus fibrosus (AF) or through the thickness of the AF. Work by Iatridis et al highlighted spatial variations in biochemical composition of mild to moderately degenerate human discs.²⁰ Specifically, a linear decrease in water and proteoglycan content was observed from the inner AF to the outer AF, and NP was reported as being more heterogeneous than previously thought. Similar analyses have been performed to quantify the spatial variation in bovine disc composition; however, these analyses have been limited in either spatial resolution or quantitative power. That is, only large, discreet disc regions have been considered, such as comparing the NP with the AF or the inner AF with the outer AF.^{2,5,6} Other studies observed radial variations in tissue composition with high spatial resolution using histology and immunohistochemistry, but these techniques were limited in their ability to provide absolute, quantitative values.^{8,10} More recently, Emanuel et al reported variations in disc composition with high spatial resolution using Fourier-transform infrared imaging, but this method only reports relative compositional changes in arbitrary units.²²

Despite the extensive use of bovine caudal discs in spine research, the radial variations in bovine disc composition have not yet been

rigorously quantified with high spatial resolution. Thus, the first objective of this study was to provide absolute quantitative measurements of biochemical composition of bovine caudal discs with significantly increased spatial resolution using traditional biochemical techniques. The second objective was to quantify the spatial distribution of free and bound water content in the disc using Raman spectroscopy with differential scanning calorimetry. The final objective was to simultaneously image collagen fibers and lipid droplets throughout the disc using multi-modal imaging techniques (CARS and SHG).

2 | MATERIALS AND METHODS

2.1 | Sample preparation

Fresh bovine caudal spine sections were acquired from a local butcher and stored at -20°C (20 spines, age = 18–24 months). Caudal spines were thawed at room temperature and surrounding musculature and ligaments were removed with a scalpel. Tails were then hydrated in 0.15 M phosphate-buffered saline solution (PBS) for 18 hours at 4°C to ensure that each specimen and spine experience similar hydration histories prior to performing biochemical analyses.²³ Once hydrated, intervertebral discs were removed from the top two levels with a scalpel ($n = 38$, Levels C1–C3), wrapped in PBS-soaked gauze, and stored at -20°C for biochemical analyses. The number of specimens used for each individual test is provided in the supplemental material (Table S1).

2.2 | Biochemical analysis

Ten discs were randomly chosen and used for traditional biochemical analyses. Discs were removed from the freezer and placed on a freezing stage microtome (-16°C) to prepare specimens of concentric rings (Figure 1). First, the average disc diameter was measured with digital calipers to estimate the approximate thickness of each layer (10 total layers). The first layer was taken from the center of the NP, as a solid

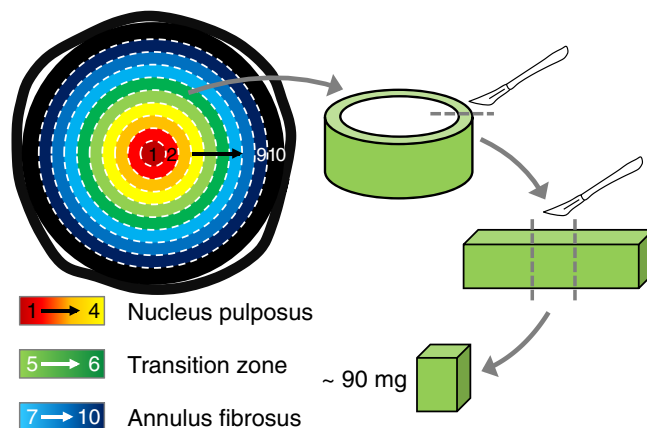


FIGURE 1 Schematic of sample preparation. A 4 mm cylindrical tissue was removed from the center of the disc (Layer 1). Then, concentric layers of equal thickness were obtained (Layers 2–10). A ~90 mg tissue strip was collected from each layer for analysis

cylinder, using a biopsy punch (4 mm diameter). Subsequent layers were removed as hollow cylinders with wall thickness of ~1 mm. For inner layers, biopsy punches with diameters of 6 to 10 mm were used to create concentric cylinders. Then, a scalpel was used to create concentric cylinders for the outer layers (diameter ~12-20 mm). Each hollow cylinder was cut and laid flat. Then, a rectangular tissue sample with a wet weight (WW) of approximately 90 mg was cut from the tissue strip (Figure 1). We assumed that bovine disc composition along the circumference was consistent. Samples were then freeze-dried in a lyophilizer for 48 hours and re-weighed to obtain dry tissue weight (DW). Water content was calculated as the difference between wet and dry weights divided by wet weight (ie, $[WW - DW]/WW$). Each freeze-dried sample was digested in 1 mL of 2 mg/mL proteinase-K solution at 56°C for 24 hours.

Proteinase-K tissue-digests were used to measure sulphated glycosaminoglycan (s-GAG), collagen, and DNA contents. s-GAG content was measured using the 1,9-dimethylene blue dye-binding (DMMB) assay.²⁴ Total collagen content was measured using the ortho-hydroxyproline (OHP) colorimetric assay and assuming a 1:7.5 OHP-to-collagen mass ratio.²⁵ DNA content was determined using the PicoGreen fluorescence assay (Molecular Probes, Eugene, Oregon). Collagen, s-GAG, and DNA measurements were normalized to wet and dry tissue weights to account for variations in initial tissue hydration and to compare results across data reported in the literature.

2.3 | Swelling ratio

Eight additional discs were used to evaluate bovine disc swelling properties. Tissue samples were prepared and weighed as described above (ie, ~90 mg specimens). Each sample was immersed in 10.0 mL of 0.15 M PBS and allowed to freely swell for 16 hours at room temperature (~23°C). After free swelling, samples were gently blotted and re-weighed to obtain the tissue's swollen weight (SW). The swelling ratio was calculated as the difference between the swollen weight and initial wet weight normalized by the initial wet weight (ie, $[SW - WW]/WW$). A 1 mL aliquot of swelling solution was saved to determine whether s-GAGs leached into the PBS solution during swelling. Swollen samples were digested using proteinase-K, and s-GAG contents of tissue digests and swelling solutions were measured using the DMMB assay.

2.4 | Raman spectroscopy

All Raman spectroscopic measurements were collected at room temperature (excitation at 632.8 nm; Horiba Jobin Yvon Labram spectrometer with Olympus BX41 confocal microscope). Spectra were recorded over a wide frequency range (0-3800 cm^{-1}) for points located in the NP and AF ($n = 3$ discs). Raman data were post-processed by performing a baseline correction using a piecewise linear fitting and smoothed using a Savitzky-Golay filter. To compare across different regions, spectra were normalized to have the same intensity signal at 2945 cm^{-1} , which corresponded to the strongest CH vibrational line. Representative spectra for the NP and the AF were

obtained by averaging 12 spectra taken from each region. The low frequency region ($<300 \text{ cm}^{-1}$) was excluded from the spectra, due to the high signal intensity from the Rayleigh line.²⁶

A narrower range of spectra data (2700-3800 cm^{-1} range) was collected for 10 bovine discs to measure radial distribution of water-to-protein content. Measurements were taken at inner NP (i-NP), outer NP (o-NP), inner AF (i-AF), and outer AF (o-AF). Discs were freeze-dried for 72 hours, and measurements were repeated on dry discs to measure the decrease in water content associated with removal of free water molecules.²⁷ Specifically, water-to-protein content of wet and dry discs was determined by taking the ratio of integrated areas of OH and CH bands (3050-3800 cm^{-1} and 2800-3050 cm^{-1} , respectively), which is directly proportional to the relationship between water and protein/lipid molecules.²⁸ Raman-based water-to-protein ratios were compared to data collected from traditional biochemical analysis (ie, water content/[collagen + s-GAG content] with respect to the tissue's wet weight). The average of two adjacent layers from the biochemical analysis was used to estimate water-to-protein ratios for each region (ie, i-NP: layers 1-2, o-NP: layers 3-4, i-AF: layers 7-8, and o-AF: layers 9-10). The percentage of bound water with respect to total water content was estimated by comparing water-to-protein ratios from dry and wet samples.

2.5 | Differential scanning calorimetry analysis

Differential Scanning Calorimetry (DSC) measurements were acquired on inner NP and outer AF tissue samples collected from seven bovine caudal discs (Mettler Toledo Model DSC 1, Star^e system). Specifically, wet tissue samples, 5 to 15 mg, were obtained with a scalpel and hermetically sealed in aluminum pans. Weights of tissue samples and sealed pans were measured before and after the test (NewClassic MS, Mettler Toledo; accuracy resolution = ± 0.0001 mg). Prior to DSC measurements, pans were pierced to allow water evaporation during testing. Samples were cooled to -30°C and held at -30°C for 15 minutes to allow water in the tissue to freeze (heating/cooling rate = $10^\circ\text{C}/\text{min}$). Then, samples were heated to 180°C , and dried at 180°C for 30 minutes to determine mass lost during heating (m_{loss} ; Figure 2A). Mass loss was reported as a percentage of initial tissue mass.

Crystallization temperature (T_c) was defined as the peak exothermic temperature (eg, Figure 2A—peak near -10°C). Crystallization enthalpy (ΔH_c) was calculated as the area under the exothermic peak. The onset temperature of melting ($T_{m,\text{onset}}$) was defined as the temperature at which the extrapolated baseline intersected with the tangent line of the linear region from the melting curve during endothermic reaction (Figure 2B—dashed red lines).²⁹ Maximum melting temperature ($T_{m,\text{max}}$) was defined as the peak temperature during melting. The latent heat of melting (ΔH_m) was calculated by finding the area under the melting peak (between temperatures -20°C and $+15^\circ\text{C}$; Figure 2B—shaded area). The amount of freezable water was calculated by dividing the latent heat of melting (ie, ΔH_m) by the melting enthalpy of pure ice (330 J/g). The presence of a second endothermic phenomenon (temperatures $>60^\circ\text{C}$) has been associated

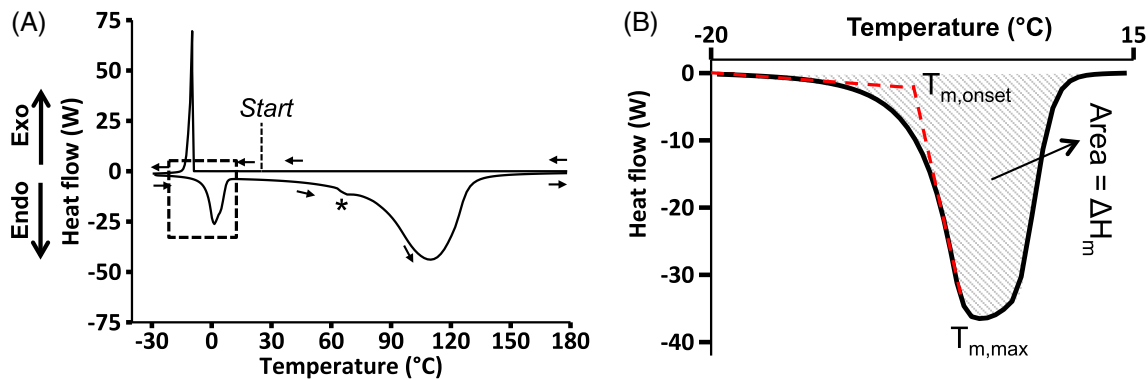


FIGURE 2 (A) Representative DSC curve. Negative heat flow values represent an endothermic response, while positive heat flow values represent an exothermic response. (B) Detail from dashed boxed in Figure 2A showing onset temperature of melting ($T_{m,onset}$), maximum temperature of melting ($T_{m,max}$), and latent heat of melting (ΔH_m), which was calculated as the area under the curve between -20°C and $+15^\circ\text{C}$

with collagen denaturation.³⁰ The onset ($T_{d,onset}$) and maximum temperature ($T_{d,max}$) of the denaturation curve were determined using the methods described above for melting parameters.

2.6 | Multimodal nonlinear optical imaging

Collagen fibers and lipid droplets were simultaneously imaged using a multimodal CARS and Second Harmonic Generation (SHG) microscopy system. A femtosecond optical parametric oscillator (OPO), with dual output (Insight DS+, Spectra-Physics, Santa Clara, California) was used as the excitation source and coupled into the inverted laser-scanning microscope chassis (FV1200, Olympus, Waltham, Massachusetts). One output was tunable, and the other was fixed at 1040 nm. Imaging was performed using a 60x water immersion objective lens (UPLSAPO60XWIR, Olympus). Lipid droplets were imaged with CARS by tuning the pump beam to 802 nm, such that the beat frequency between the pump line and the fixed Stokes line at 1040 nm matched the CH_2 stretching vibration of $\sim 2850\text{ cm}^{-1}$. Collagen fibers were visualized using the SHG and sum-frequency generation (SFG) signals. Both signals were collected in the epi-direction and separated from the excitation lasers by a shortpass 690 nm dichroic mirror. The CARS and SHG/SFG signals were further separated by a shortpass 570 nm dichroic mirror, and both signals were collected simultaneously by two external photomultiplier tubes. The SHG signal comprised the combined contribution of the second harmonics of the pump and Stokes beams respectively, as well as their sum-frequency signal.

Bovine caudal discs ($n = 3$ discs from C1C2 or C2C3) were isolated from freshly acquired tails, and used for multimodal imaging. A mid-sagittal slice was cut from each disc and placed onto a glass coverslip (0.17 mm thickness) for imaging. Multiple images (image resolution: $212 \times 212\ \mu\text{m}$) were collected on the same sample at inner NP (i-NP), outer NP (o-NP), inner AF (i-AF), and outer AF (o-AF). Two-color images were produced using Matlab (Mathworks, Inc.) to highlight collagen fibers (purple) and lipid droplets (green). The area and count of lipid droplets were estimated from 2D binary images using ImageJ. The relative change in SHG signal intensity was used as a marker for characterizing radial distribution of collagen in bovine discs. To

quantify collagen content for each tissue region, the mean signal intensity was calculated and normalized by the applied voltage from the photomultiplier tube. Collagen content of the inner NP, outer NP, and inner AF were reported relative to collagen content of the outer AF.

2.7 | Statistical analysis

All statistical analyses were performed in R (R Project for Statistical Computing, Vienna, Austria). Exploratory data analysis indicated the presence of non-normal distributions; hence, data were reported with median values, unless stated otherwise, and non-parametric statistical analyses were preferred over parametric analyses. Significance was assumed at $P < .05$ for all statistical analyses.

For traditional biochemical analyses, disc regions were defined a priori based on visual inspection of the NP and AF boundary, where layers 1 to 4 represented the NP, layers 5 to 6 were in the transition region between the NP and AF, and layers 7 to 10 represented the AF (Figure 1). The Kruskal-Wallis test, followed by Mann-Whitney U pairwise comparison tests, was conducted to determine within-region differences in properties. Pairwise comparisons were only conducted to detect differences within each tissue region (ie, within NP or AF layers). Additionally, a Mann-Whitney U test was performed to compare biochemical properties between the NP and AF by pooling data from each region (layers 1-4 for NP and layers 7-10 for AF). A Bonferroni correction was used to account for multiple comparisons.

A two-way analysis of variance (ANOVA), followed by post-hoc analysis with Holm-Bonferroni correction, was performed to evaluate differences in water-to-protein ratios measured by the traditional biochemical analysis and Raman spectroscopy (factors = disc region and measurement method). A similar analysis was conducted to compare relative collagen content distribution from the normalized SHG signal and traditional biochemical analysis. For DSC data, a Mann-Whitney U test was performed to compare NP and AF thermal properties. Median and interquartile range values were reported for each thermal property.

3 | RESULTS

3.1 | Traditional biochemical assays

Water and s-GAG contents were relatively constant throughout the NP (ie, layers 1-4), except the water content of layer 1, which was significantly greater than the water content of layers 3 and 4 ($P < .05$; Figure 3A,B). No other differences in NP water content ($P \geq .3$) or NP s-GAG content were observed ($P \geq .8$; Figure 3C,D). In contrast, both water and s-GAG contents decreased from the inner AF to the outer AF (ie, from layer 7-10; Figure 3). Overall, NP s-GAGs accounted for 30% to 36% of the tissue's dry weight (ie, 300-360 mg/g) or 6% by wet weight (ie, 60 mg/g). In the AF, s-GAGs accounted for 5% to 20% of the tissue's dry weight (ie, 50-200 mg/g) or 1% to 5% by wet weight (ie, 10-50 mg/g; Figure 3C,D). The water to s-GAG ratio did not change significantly within the NP; however, the water to s-GAG ratio of layer 10 was significantly greater than that of the inner AF layers (ie, layers 7-8, $P < .05$; Figure 4).

Collagen accounted for 28% to 47% of the NP's dry weight (ie, 280-470 mg/g) or 4% to 9% by wet weight (ie, 40-90 mg/g). In the AF, collagen accounted for 58% to 80% of the tissue's dry weight (ie,

580-800 mg/g) or 14% to 29% by wet weight (ie, 140-290 mg/g—Figure 5A,B). Collagen content normalized by dry weight in the outer AF was 2.5-fold greater than the collagen content at the disc center (6.6-fold difference when normalized by wet weight; Figure 5A,B). However, no statistically significant differences were detected between layers in the NP or AF when collagen content was normalized by dry tissue weight (Figure 5A). Conversely, normalizing collagen content by wet weight indicated a statistically significant difference between layers 7 and 10 ($P = .01$; Figure 5B).

DNA content normalized by both dry and wet tissue weight was relatively consistent from the NP to the inner AF (Figure 5C, D). The median NP DNA content was 270 $\mu\text{g/g}$ DW or 48 $\mu\text{g/g}$ WW. Although DNA content was relatively constant from the NP to the inner AF, the median DNA content was higher in the outermost layer (Layer 10—607 $\mu\text{g/g}$ DW or 209 $\mu\text{g/g}$ WW; Figure 5C,D).

3.2 | Swelling ratio

The swelling ratio decreased from 1.85 at the disc center to 0.5 in the outer AF, which represents a 185% increase in NP tissue mass and a 50%

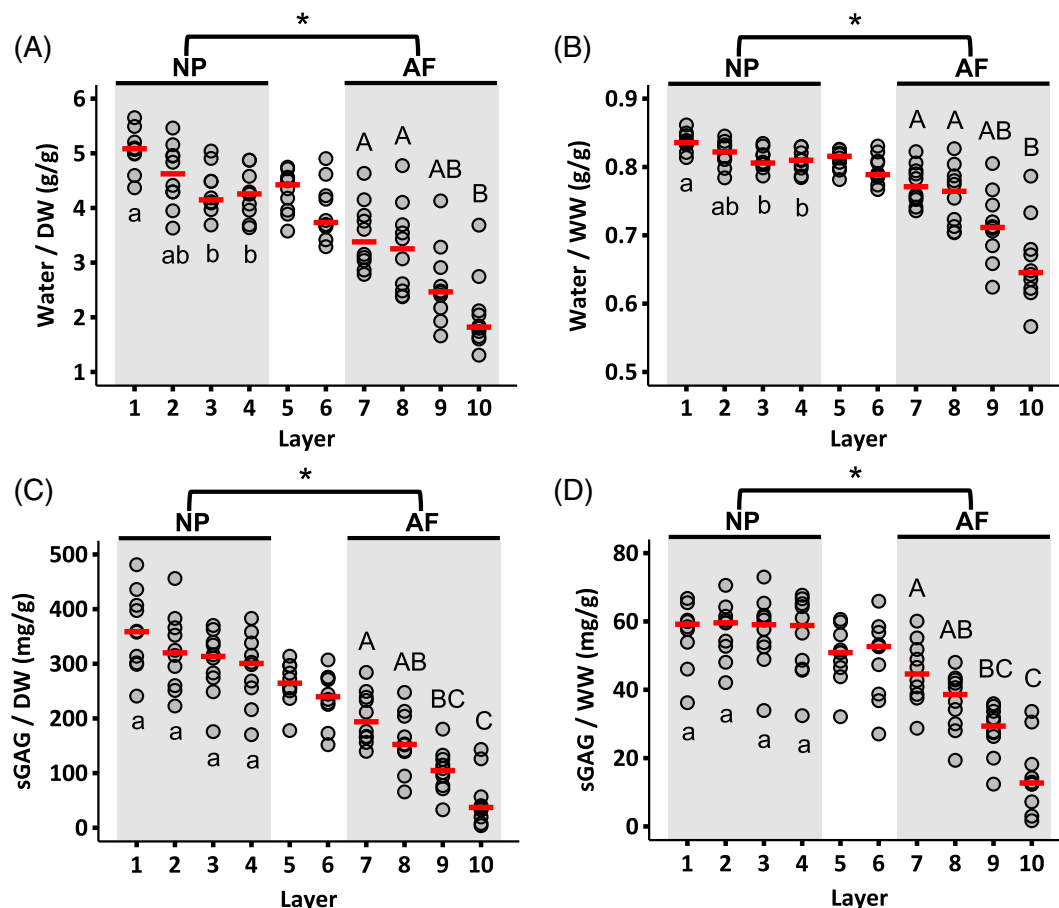


FIGURE 3 Radial distribution of water content normalized by (A) dry weight (DW) and (B) wet weight (WW). Radial distribution of sulfated GAG content normalized by (C) dry weight and (D) wet weight. Circles indicate individual data and red dashes indicate median values for each layer. NP and AF biochemical properties were compared using a Mann-Whitney U test on pooled data from Layers 1-4 (NP) and Layers 7-10 (AF; * represents $P < .05$). Differences in biochemical composition within each region (ie, shaded areas) were assessed using a Mann-Whitney U test with Bonferroni correction. Layers that do not share the same letter are significantly different ($P < .05$)

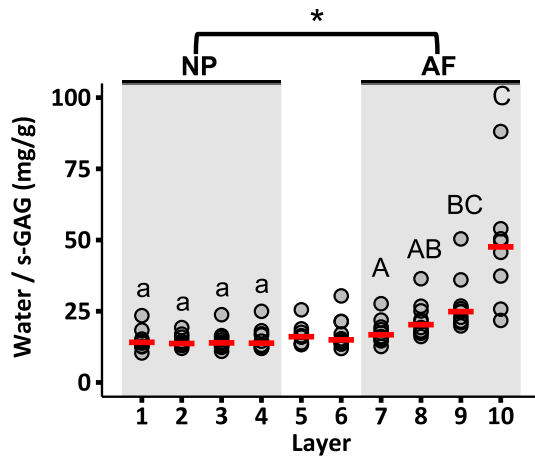


FIGURE 4 Radial distribution of water content normalized by sulfated GAG content. Circles indicate the individual data and red dashes indicate the median values. Values >100 in the last layer were omitted for clarity ($n = 2$ omitted values). NP and AF biochemical properties were compared using a Mann-Whitney U test on pooled data from Layers 1-4 (NP) and Layers 7-10 (AF; * represents $P < .05$). Differences in biochemical composition within each region (ie, shaded areas) were assessed using a Mann-Whitney U test with Bonferroni correction. Layers that do not share the same letter are significantly different ($P < .05$)

increase in outer AF tissue mass with swelling (Figure 6A). s-GAG leaching from tissue specimens was observed during free-swelling and the amount of leached s-GAGs was greater for the NP compared to the AF ($P < .001$ for NP vs AF; Figure 6B). s-GAG leakage corresponded to ~50% of the total s-GAG in the NP and ~30% of the total s-GAG in the AF (Figure 6D).

3.3 | Raman spectroscopy

Raman spectra peaks were similar for the NP and AF, with sharp peaks at 863, 940, 1252, 1455, and 1661 cm^{-1} . Bands associated with amino acids and lipids dominated the spectral fingerprint for both regions (Figure 7A— $<1800 \text{cm}^{-1}$). Bands located at 2800 to 3020 cm^{-1} were associated with stretching modes of CH_2 and CH_3 , while bands at 3020 to 3800 cm^{-1} were associated with total water content (ie, free and bound water; Figure 7A). Moreover, the water spectrum was complex and exhibited contributions from multiple smaller peaks.

The water-to-protein ratio was 7.5 at the disc center and decreased from the center of the disc to the outer AF ($P < .001$; Figure 7B,C). Importantly, the water-to-protein ratios of the inner NP and outer NP were significantly different ($P = .012$).

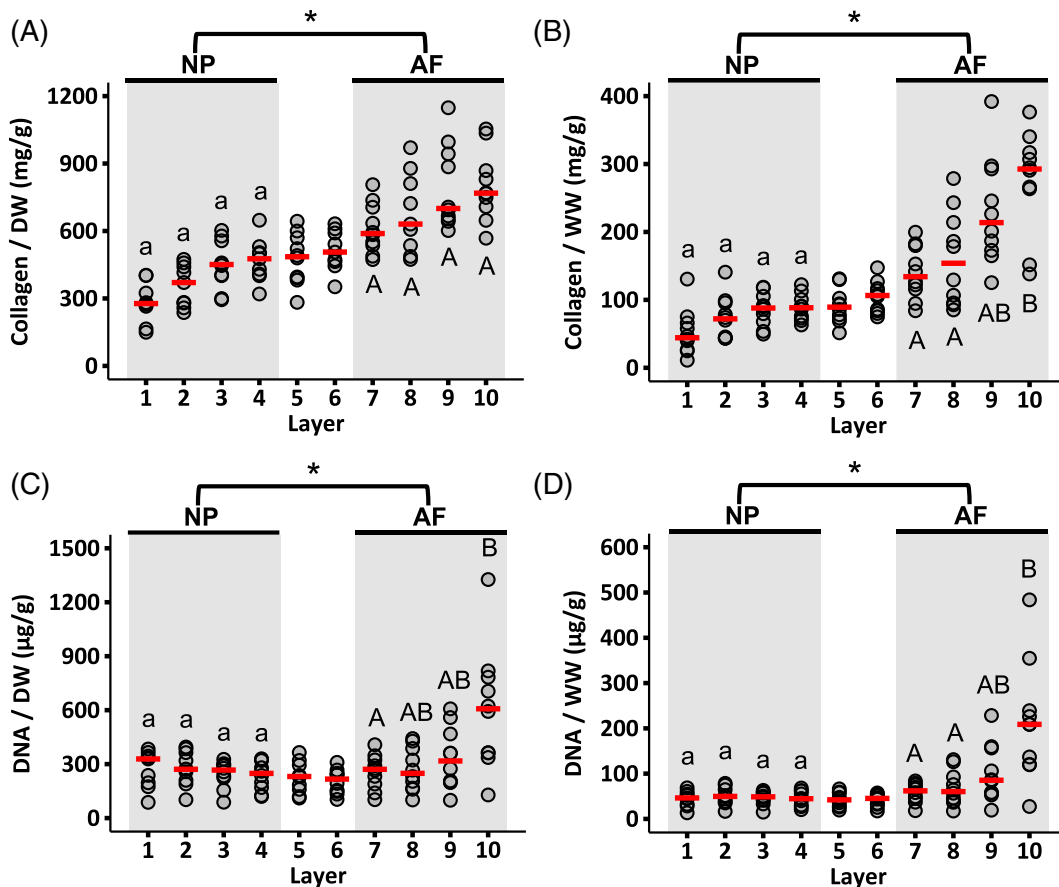


FIGURE 5 Radial distribution of collagen content normalized by (A) dry weight and (B) wet weight. Radial distribution of DNA content normalized by (C) dry weight and (D) wet weight. Circles indicate the individual data and red dashes indicate the median values. NP and AF biochemical properties were compared using a Mann-Whitney U test on pooled data from Layers 1-4 (NP) and Layers 7-10 (AF; * represents $P < .05$). Differences in biochemical composition within each region (ie, shaded areas) were assessed using a Mann-Whitney U test with Bonferroni correction. Layers that do not share the same letter are significantly different ($P < .05$)

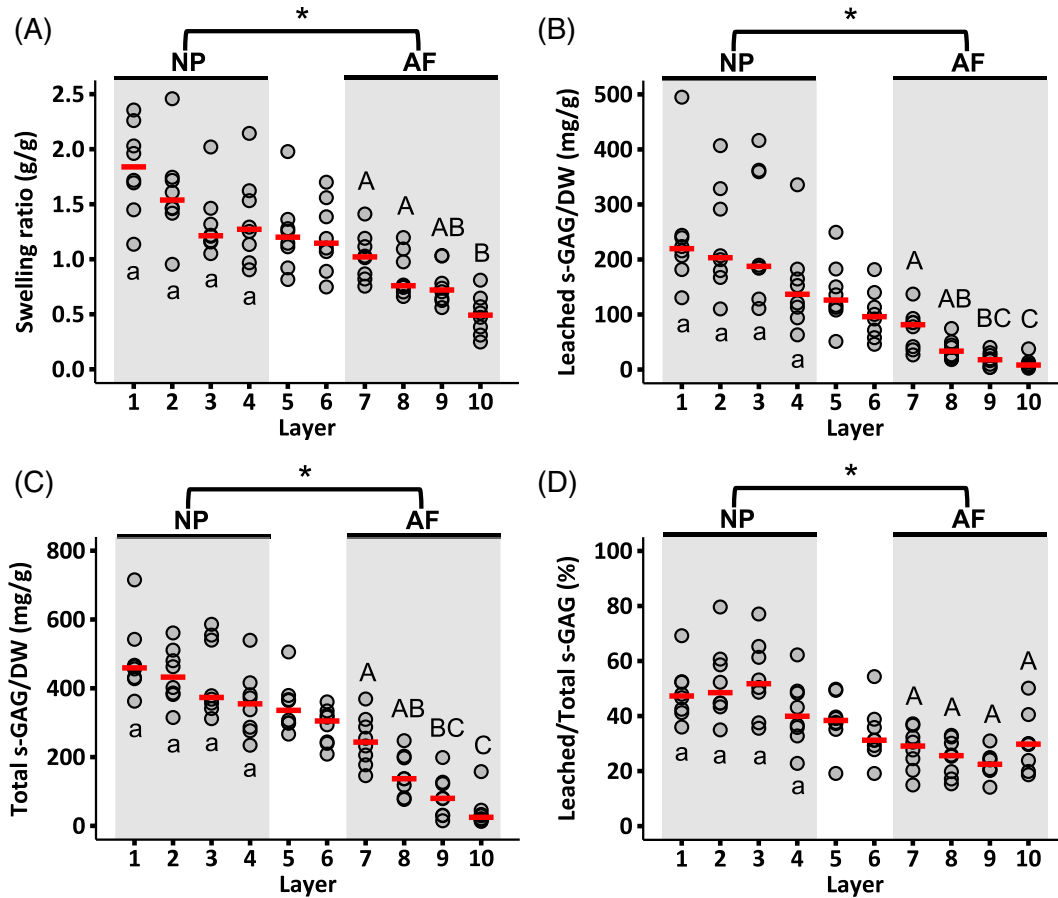


FIGURE 6 Radial distribution of (A) swelling ratio, (B) s-GAGs leached into the swelling solution normalized by dry weight, (C) total s-GAG normalized by dry weight, and (D) leached s-GAG normalized by total s-GAG. Circles indicate individual data and red dashes indicate median values. NP and AF biochemical properties were compared using a Mann-Whitney U test on pooled data from Layers 1-4 (NP) and Layers 7-10 (AF; * represents $P < .05$). Differences in biochemical composition within each region (ie, shaded areas) were assessed using a Mann-Whitney U test with Bonferroni correction. Layers that do not share the same letter are significantly different ($P < .05$)

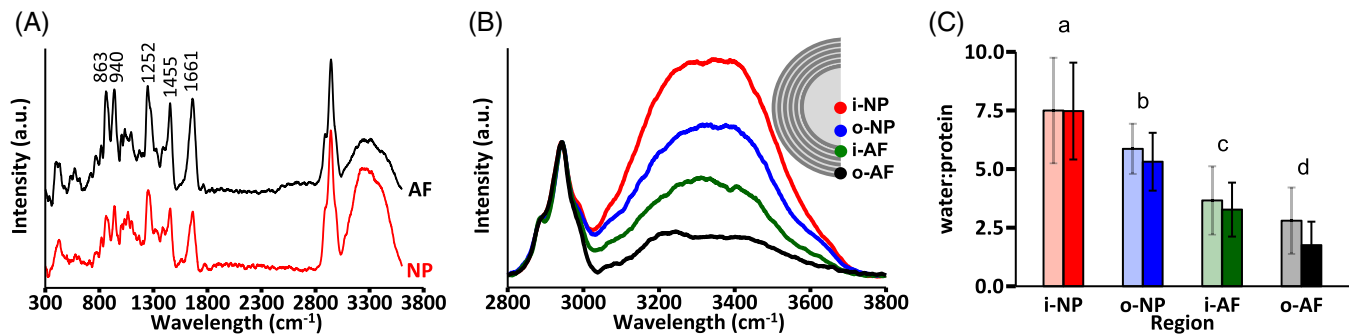


FIGURE 7 (A) Representative Raman spectra for nucleus pulposus (NP) and annulus fibrosus (AF) specimens. (B) Spectra from four regions within the disc to assess water content distribution, and (C) comparison of water-to-protein ratios collected from Raman spectroscopy (dark bars) and traditional biochemical analysis (light bars; two-way ANOVA - $P = .09$ for measurement method and $P = .001$ for disc region). Pairwise comparisons were performed using t-tests with Holm-Bonferroni correction. Layers that do not share the same letter are significantly different ($P < .05$)

Furthermore, the water-to-protein ratios obtained from Raman spectra agreed well with measurements from traditional biochemical assays (Figure 7C—solid vs light bars; two-way ANOVA: $P = .09$ for measurement method and $P = .001$ for disc region). The absolute

amount of bound water content did not depend on disc region ($P = 1.0$; Figure 8A), however, bound water accounted for 3% of the total water content in the NP and 11% of the total water content in the outer AF (Figure 8B).

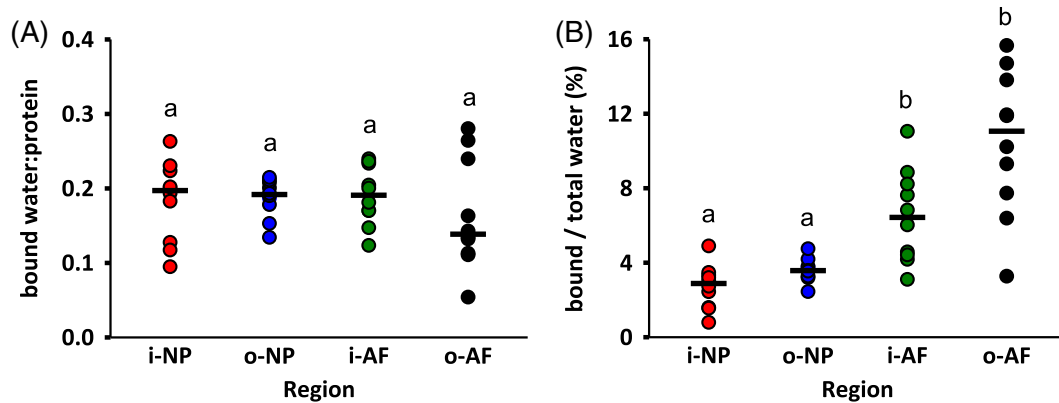


FIGURE 8 (A) Bound water content normalized by total protein content, and (B) percentage of bound water content with respect to total water content. Circles indicate the individual data and black dashes indicate the median values. Changes in biochemical composition were determined by performing Kruskal-Wallis test followed by pairwise comparisons using Mann-Whitney U test with Bonferroni correction. Layers that do not share a letter are significantly different ($P < .05$)

3.4 | DSC analysis

The endothermic peak observed between -20°C and $+10^{\circ}\text{C}$ was associated with melting of ice, and the peak between 80°C and 150°C was associated with possible denaturation of tissue collagen (Figure 2A). There were no obvious differences in crystallization temperature (T_c), onset temperature of melting ($T_{m,onset}$), maximum melting temperature ($T_{m,max}$), onset temperature of denaturation ($T_{d,onset}$), and maximum denaturation temperature ($T_{d,max}$) between the NP and AF ($P \geq .09$; Table 1). However, enthalpy of crystallization (ΔH_c) and latent heat of melting (ΔH_m) were greater in the NP than the AF (Table 1). The median latent heat of melting in the NP was 246 J/g, indicating that 75% of the water in the NP was freezable water (ie, $\Delta H_m / \Delta H_{m, \text{pure ice}}$). In contrast, the average amount of freezable water in the AF was 65%.

Collagen denaturation was observed at temperatures as low as 65°C , while the maximum temperature of denaturation ($T_{d,max}$) occurred near 110°C (Figure 2A). The denaturation curve of the samples exhibited a small kink at lower temperatures (65°C – 70°C ; * in Figure 2A). Heating specimens above T_d resulted in more than 70% tissue mass loss (0.82 g/g WW loss in the NP and 0.71 g/g WW loss in the AF—Table 1).

3.5 | Multimodal nonlinear optical imaging

Multimodal images showed fiber architecture and the presence of lipid deposits in the disc (Figure 9A). The relative change in the SHG signal intensity throughout the disc was similar to the relative change in collagen content observed from the OHP assay (Figure 9B; two-way ANOVA: $P > .9$ for measurement method and $P < .001$ for disc region). Lipid deposits were distributed equally throughout the disc and appeared either as a single droplet or as clusters of small droplets (Figure 9C). However, there were noticeable differences between discs used for imaging lipids. That is, two of the three discs had a large amount of lipid droplets, while one disc had few to no lipid droplets. The distribution of lipid droplet area was highly skewed, such that

80% of lipid droplets were smaller than $5 \mu\text{m}^2$ (diameter $\approx 2.5 \mu\text{m}$), while the largest droplets had an area of $\sim 230 \mu\text{m}^2$ (diameter $\approx 17 \mu\text{m}$).

4 | DISCUSSION

In this study, several measurement techniques were used to characterize radial variations in biochemical composition of bovine caudal discs. Specifically, water, sulfated GAGs, collagen, and DNA contents were measured with traditional biochemical assays to obtain quantitative measurements. Gravimetric water content was compared to measurements from Raman spectroscopy and DSC. Combined CARS and SHG microscopy was used to visualize lipids within the collagen fiber network, and explore the potential use of SHG imaging for measuring relative collagen content in the disc.

Most numerical studies describe the NP as a homogeneous isotropic material, whereas the AF is often described as a heterogeneous material.^{31–33} The results of the current study showed that the water content and water-to-protein ratio of the inner NP were greater than the values measured for the outer NP. Meanwhile, the swelling capacity (ie, swelling ratio), collagen content, and DNA content were constant throughout the NP. In contrast, the AF exhibited radial variations in all biochemical properties. Water and s-GAG contents decreased, while collagen content increased from the inner AF to the outer AF, and our findings agreed well with previous studies.^{2,6,34,35} Lastly, swelling capacity throughout the disc depended on the initial s-GAG content, where NP explants experienced higher swelling ratios than AF explants.^{36,37}

Knowledge of cell density in healthy native tissues is important for regenerative medicine strategies that aim to inject stem cells or implant cell-based engineered tissues for disc repair.³⁸ The DNA content was constant throughout the NP, but increased nonlinearly across the AF. DNA content throughout the majority of the AF (ie, layers 7–9) was comparable to NP DNA content ($<100 \mu\text{g/g WW}$). However, there was a 2-fold increase in DNA content in the

TABLE 1 NP and AF values from differential scanning calorimetry

Region	T_c (°C)	ΔH_c (J/g)	$T_{m,onset}$ (°C)	$T_{m,max}$ (°C)	ΔH_m (J/g)	$T_{d,onset}$ (°C)	$T_{d,max}$ (°C)	m_{loss} (g/g)	WC (g/g)
NP	-12.8 (-13.8, -11)	303* (284, 319)	-4.0 (-4.2, -3.1)	1.7 (1.4, 2.8)	246* (236, 255)	97 (87, 99)	106 (104, 107)	0.82* (0.80, 0.83)	0.75* (0.71, 0.77)
AF	-12.7 (-16.9, -9.2)	205* (181, 266)	-3.7 (-3.8, -3.1)	4.2 (3.2, 5.0)	214* (193, 218)	89 (81, 97)	110 (107, 119)	0.71* (0.68, 0.73)	0.65* (0.59, 0.66)

Note: Data are expressed as median (interquartile range).

Abbreviations: AF, annulus fibrosus; m_{loss} , mass loss; NP, nucleus pulposus; T_c , crystallization temperature; $T_{d,max}$, maximum denaturation temperature; $T_{d,onset}$, onset temperature of denaturation; $T_{m,max}$, maximum melting temperature; $T_{m,onset}$, onset temperature of melting; WC, water content; ΔH_c , crystallization enthalpy; ΔH_m , latent heat of melting.
*Significant differences between NP and AF (Mann-Whitney U test, $P < .05$).

outermost AF layer. The increase in DNA content at the outer AF was most likely due to greater access to nutrients from surrounding blood vessels and connective tissues.³⁹

Similar to human disc tissue explants, bovine tissue explants released s-GAGs into the solution during swelling, where a greater percentage of s-GAGs was released by tissues with a greater initial s-GAG concentration (ie, the NP).³⁷ Region-specific differences in tissue properties, such as permeability, collagen architecture, and the size and distribution of proteoglycan molecules, likely account for differences in swelling properties between the NP and AF, as well as throughout the AF.^{37,40,41} Furthermore, s-GAG leakage may increase as effective pore size increases with swelling.⁴¹ Importantly, GAGs are thought to primarily contribute to compressive mechanics, but recent work has highlighted the importance of GAGs in AF tensile mechanics.^{42,43} Thus, GAG loss during long duration tests may affect tissue mechanics, particularly during tests that may include partial or full recovery in an aqueous solution.

To the best of our knowledge, the spatial distribution of lipids within the disc collagen network has not been presented. Hence, multimodal microscopy was used to obtain a quick simultaneous imaging of collagen fibers and lipid droplets without the need of external dyes or fixatives, as used for histology. Images confirmed the presence of lipid droplets.⁴⁴ Lipids appeared throughout the disc, either as isolated spheres or as clusters, and the majority of droplets were smaller than ~1.5 μm in diameter. Lipids have also been observed in other collagen-rich connective tissues, and various factors, such as age, degeneration, diet, and exercise, have been reported to influence lipid concentration.⁴⁵⁻⁴⁸ This study only evaluated lipid content in healthy discs, but it is possible that age and disease will affect the lipid concentration in the disc, based on observations in cartilage and tendon.^{45,49} Additional work is needed to understand the role and concentration of lipids throughout the disc with aging, degeneration, and diseases.

Raman spectroscopy has been used to investigate biochemical composition of various tissues, including cartilage, bone, skin, and brain,⁵⁰⁻⁵⁴ but there has been little to no work on the intervertebral disc. Similar to observations in other tissues, Raman spectra of bovine discs were dominated by vibrational bands from structural proteins and lipids. As expected, there were similarities between NP and AF spectra, due to similarities in tissue composition (ie, water, s-GAG, and collagen content). Raman spectra of the bovine disc exhibited sharp peaks at 863, 940, 1252, 1455, and 1661 cm^{-1} . Peaks at ~860 and ~940 cm^{-1} have been previously identified as a marker for C-C stretching vibrational mode of proline and hydroxyproline residues in collagen.^{55,56} Bands with a peak at 1252 and 1661 cm^{-1} have been associated with amide III and amide I, respectively, where amide I mainly reflects the C=O stretching vibration and the amide III band has contributions from several chemical bonds.^{57,58} In biological tissues, amide bands have been primarily used to study age- and disease-related alterations in protein secondary structure and conformation.^{57,59,60} The peak at ~1455 cm^{-1} corresponds to deformation vibrations of CH_2 and CH_3 amino acid side chains and lipids.²⁶ It should be noted that Raman vibrations have been related to more

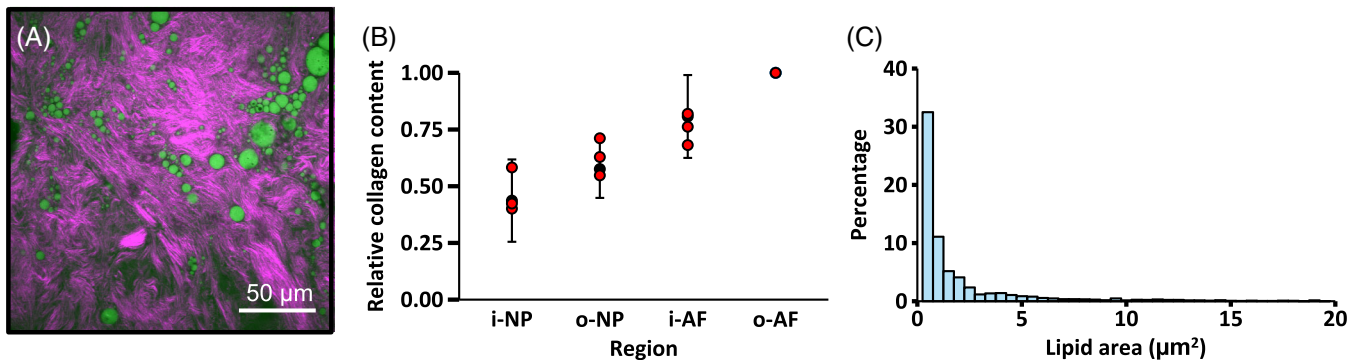


FIGURE 9 (A) Combined image from SHG (purple) and CARS (green, 2850 cm^{-1}) imaging. (B) Collagen content at the inner NP (i-NP), outer NP (o-NP), and inner AF (i-AF) normalized by collagen content of the outer AF (o-AF). Red circles represent SHG measurements, while black error bars represent mean \pm standard deviation from the OHP assay. (C) Distribution of lipid droplet area throughout the disc obtained using the pooled data from the NP and AF. Data from lipids with areas greater than $20\text{ }\mu\text{m}^2$ ($\sim 2\%$) are not shown for clarity

than one amino acid or chemical group, making it difficult to identify differences in the fingerprint region. Hence, only predominant peak locations were reported and compared between disc regions.

In contrast, differences in the high-frequency region (ie, $>2800\text{ cm}^{-1}$) were easily identifiable and used to determine radial distributions of bound and free water (sometimes referred to as “mobile” or “freezable” water).^{27,61–63} While freeze- or air-drying tissue specimens is frequently used to remove free water molecules, removal of bound water is more difficult, requiring drying under very low pressures and high temperatures or chemical treatments (eg, acetone or ethanol).^{27,64} Hence, water content values commonly reported only refer to the amount of free water in the tissue.^{18,20,65} We measured the contribution of bound water to the total water content by evaluating changes in Raman spectra after freeze-drying. Our finding suggests that only a small portion of the total water content is bound to macromolecules in the matrix (ie, proteoglycans and collagen; 3% in the NP and 11% in the AF, Figure 8B). Thus, the majority of water molecules are mobile and free to diffuse out of the disc during loading or dehydration. The relative bound water content in the NP agreed well with reported values for cartilage ($\sim 4\%$),^{27,66} but the concentration of bound water in the NP and AF was lower than the concentration measured for bovine pericardium, skin, and muscle (25%–40%).^{30,62,67}

Thermal properties of the bovine disc were determined to identify temperatures associated with water freezing and melting, and collagen stability. The second endothermic peak, observed to start at temperatures as low as 65°C , is associated with collagen denaturation, where interchain hydrogen bonds rupture, causing irreversible damage to the collagen structure.^{30,68} Denaturation temperatures for the NP and AF were similar to each other and to other biological tissues, such as bovine pericardium, rat-tail tendon, and human skin.^{30,62,69} The small kink observed between 65°C and 70°C (Figure 2—“*”) has been associated with cleavage of weak bonds between water and matrix macromolecules or conformational changes within fibrils (eg, partial fibril shrinkage), rather than breaking of stronger bonds, which occurs at a slightly higher temperature ($\sim 80^\circ\text{C}$).^{70,71}

This study is not without its limitations. First, there was high variability in measured properties despite our attempts to minimize potential sources for variation (eg, pre-hydrating tails to provide similar hydration history for each specimen). Second, we only measured major proteins found in the disc. For example, the NP and inner AF are comprised of mostly type II collagen, while the outer AF contains predominantly type I collagen.¹⁸ It is also known that other types of collagen exist, as well as elastin and non-collagenous proteins.⁷² Despite the wide use of SHG microscopy for label-free imaging of collagen fibers, this technique cannot be used to visualize all types of collagens, such as collagen type III, which emits a weak SHG signal.⁷³ Third, Raman spectroscopy and multimodal imaging can be used to investigate biochemical composition at a molecular level, but assessing protein structures at that scale was not the primary focus of this work. Lastly, water was mainly referred to as being bound or free; however, the complex water spectra suggest the presence of multiple distinct water fractions as suggested in previous studies (eg, weak vs strong hydrogen bonds, free, or bulk water).^{27,74} Further analyses of the complex water spectra may provide insights into the structure of different water-protein interactions in biological tissues, particularly with respect to age- or disease-related changes.

In summary, a variety of measurement techniques were employed to characterize radial variations in bovine caudal disc biochemical composition. Traditional biochemical analyses were used to provide absolute, quantitative measurements. Furthermore, Raman spectroscopy was used to obtain radial distributions of bound water content. Some heterogeneity was observed in the NP, where the water content and water-to-protein ratio of the inner NP were greater than the outer NP. In contrast, the bovine AF exhibited a more heterogeneous distribution of biochemical properties. To better capture native tissue mechanics, computational studies should incorporate both compositional and structural heterogeneities. Furthermore, this study highlighted the potential use of less destructive techniques, such as multimodal imaging and Raman spectroscopy, to characterize biochemical composition. Comparable results between OHP assay and SHG imaging highlight the potential benefit of using SHG microscopy

as a less destructive method for measuring collagen content, particularly when relative changes are of interest. Future work will use non-destructive, label-free measurement techniques to investigate the effect of age and disease on the distribution of biochemical composition in animal and human discs.

CONFLICT OF INTEREST

The authors certify that there is no conflict of interest related to the work presented in this manuscript.

AUTHORS CONTRIBUTIONS

All authors contributed to the study design, data collection and analysis, manuscript preparation, and final approval.

ORCID

Semih E. Bezci  <https://orcid.org/0000-0002-7237-6635>

REFERENCES

- O'Connell GD, Vresilovic EJ, Elliott DM. Comparison of animals used in disc research to human lumbar disc geometry. *Spine (Phila. Pa. 1976)*. 2007;32:328-333. <https://doi.org/10.1097/01.brs.0000253961.40910.c1>.
- Beckstein JC, Sen S, Schaer TP, Vresilovic EJ, Elliott DM. Comparison of animal discs used in disc research to human lumbar disc: axial compression mechanics and glycosaminoglycan content. *Spine (Phila. Pa. 1976)*. 2008;33(6):E166-E173. <https://doi.org/10.1097/BRS.0b013e318166e001>.
- Bezci SE, Eleswarapu A, Klineberg EO, O'Connell GD. Contribution of facet joints, axial compression, and composition to human lumbar disc torsion mechanics. *J Orthop Res*. 2018a;36:2266-2273. <https://doi.org/10.1002/jor.23870>.
- Bezci SE, Klineberg EO, O'Connell GD. Effects of axial compression and rotation angle on torsional mechanical properties of bovine caudal discs. *J Mech Behav Biomed Mater*. 2018b;77:353-359. <https://doi.org/10.1016/j.jmbbm.2017.09.022>.
- Demers CN, Antoniou J, Mwale F. Value and limitations of using the bovine tail as a model for the human lumbar spine. *Spine (Phila. Pa. 1976)*. 2004;29(24):2793-2799. <https://doi.org/10.1097/01.brs.0000147744.74215.b0>.
- Showalter BL, Beckstein JC, Martin JT, et al. Comparison of animal discs used in disc research to human lumbar disc: torsion mechanics and collagen content. *Spine (Phila. Pa. 1976)*. 2012;37(15):E900-E907. <https://doi.org/10.1097/BRS.0b013e31824d911c>.
- McCann M, Séguin C. Notochord cells in intervertebral disc development and degeneration. *J Dev Biol*. 2016;4:3. <https://doi.org/10.3390/jdb4010003>.
- Boos N, Weissbach S, Rohrbach H, Weiler C, Spratt KF, Nerlich AG. Classification of age-related changes in lumbar intervertebral discs: 2002 Volvo award in basic science. *Spine (Phila. Pa. 1976)*. 2002;27(23):2631-2644. <https://doi.org/10.1097/00007632-200212010-00002>.
- Farndale RW, Sayers CA, Barrett AJ. A direct spectrophotometric microassay for sulfated glycosaminoglycans in cartilage cultures. *Connect Tissue Res*. 1982;9:247-248. <https://doi.org/10.3109/03008208209160269>.
- Pattappa G, Li Z, Peroglio M, Wismer N, Alini M, Grad S. Diversity of intervertebral disc cells: phenotype and function. *J Anat*. 2012;221:480-496. <https://doi.org/10.1111/j.1469-7580.2012.01521.x>.
- Reddy GK, Enwemeka CS. A simplified method for the analysis of hydroxyproline in biological tissues. *Clin Biochem*. 1996;29:225-229. [https://doi.org/10.1016/0009-9120\(96\)00003-6](https://doi.org/10.1016/0009-9120(96)00003-6).
- Roberts S, Evans H, Trivedi J, Menage J. Histology and pathology of the human intervertebral disc. *J Bone Joint Surg A*. 2006;88:10-14. <https://doi.org/10.2106/00004623-200604002-00003>.
- Campagnola PJ, Millard AC, Terasaki M, Hoppe PE, Malone CJ, Mohler WA. Three-dimensional high-resolution second-harmonic generation imaging of endogenous structural proteins in biological tissues. *Biophys J*. 2002;82:493-508. [https://doi.org/10.1016/S0006-3495\(02\)75414-3](https://doi.org/10.1016/S0006-3495(02)75414-3).
- Cheng J, Xie XS. Coherent anti-Stokes Raman scattering microscopy: instrumentation, theory, and applications. *J Phys Chem B*. 2004;108:827-840. <https://doi.org/10.1021/jp035693v>.
- Reiser KM, Bratton C, Yankelevich DR, Knoesen A, Rocha-Mendoza I, Lotz J. Quantitative analysis of structural disorder in intervertebral disks using second harmonic generation imaging: comparison with morphometric analysis. *J Biomed Opt*. 2007;12:064019. <https://doi.org/10.1117/1.2812631>.
- Rodríguez LG, Lockett SJ, Holtom GR. Coherent anti-Stokes Raman scattering microscopy: a biological review. *Cytom Part A*. 2006;69A:779-791. <https://doi.org/10.1002/cyto.a.20299>.
- Evans CL, Potma EO, Puoris'haag M, Cote D, Lin CP, Xie XS. Chemical imaging of tissue in vivo with video-rate coherent anti-Stokes Raman scattering microscopy. *Proc Natl Acad Sci*. 2005;102:16807-16812. <https://doi.org/10.1073/pnas.0508282102>.
- Antoniou J, Steffen T, Nelson F, et al. The human lumbar intervertebral disc: evidence for changes in the biosynthesis and denaturation of the extracellular matrix with growth, maturation, ageing, and degeneration. *J Clin Invest*. 1996;98:996-1003. <https://doi.org/10.1172/JCI118884>.
- Holzappel GA, Schulze-Bauer CAJ, Feigl G, Regitnig P. Single lamellar mechanics of the human lumbar anulus fibrosus. *Biomech Model Mechanobiol*. 2005;3:125-140. <https://doi.org/10.1007/s10237-004-0053-8>.
- Latridis JC, MacLean JJ, O'Brien M, Stokes IAF. Measurements of proteoglycan and water content distribution in human lumbar intervertebral discs. *Spine (Phila. Pa. 1976)*. 2007;32(14):1493-1497. <https://doi.org/10.1097/BRS.0b013e318067dd3f>.
- Skaggs DL, Weidenbaum M, Latridis JC, Ratcliffe A, Mow VC. Regional variation in tensile properties and biochemical composition of the human lumbar anulus fibrosus. *Spine (Phila. Pa. 1976)*. 1994;19(12):1310-1319. <https://doi.org/10.1097/00007632-199406000-00002>.
- Emanuel KS, Mader KT, Peeters M, et al. Early changes in the extracellular matrix of the degenerating intervertebral disc, assessed by Fourier transform infrared imaging. *Osteoarthr Cartil*. 2018;26:1400-1408. <https://doi.org/10.1016/j.joca.2018.06.003>.
- Bezci SE, O'Connell GD. Osmotic pressure alters time-dependent recovery behavior of the intervertebral disc. *Spine (Phila. Pa. 1976)*. 2018;43(6):E334-E340. <https://doi.org/10.1097/BRS.0000000000002354>.
- Farndale RW, Buttle DJ, Barrett AJ. Improved quantitation and discrimination of sulphated glycosaminoglycans by use of dimethylmethylene blue. *Biochim Biophys Acta*. 1986;883(2):173-177. [https://doi.org/10.1016/0304-4165\(86\)90306-5](https://doi.org/10.1016/0304-4165(86)90306-5).
- Hollander AP, Heathfield TF, Webber C, et al. Increased damage to type II collagen in osteoarthritic articular cartilage detected by a new immunoassay. *J Clin Invest*. 1994;93:1722-1732. <https://doi.org/10.1172/JCI117156>.
- Gniadecka M, Nielsen OF, Christensen DH, Wulf HC. Structure of water, proteins, and lipids in intact human skin, hair, and nail. *J Invest Dermatol*. 1998a;110:393-398. <https://doi.org/10.1046/j.1523-1747.1998.00146.x>.
- Unal M, Akkus O. Shortwave-infrared Raman spectroscopic classification of water fractions in articular cartilage ex vivo. *J Biomed Opt*. 2018;23:015008. <https://doi.org/10.1117/1.jbo.23.1.015008>.

28. Parkes M, Cann P, Jeffers J. Real-time observation of fluid flows in tissue during stress relaxation using Raman spectroscopy. *J Biomech.* 2017;60:261-265. <https://doi.org/10.1016/j.jbiomech.2017.06.004>.
29. Roos YH. Phase transitions and unfreezable water content of carrots, reindeer meat and white bread studied using differential scanning calorimetry. *J Food Sci.* 1986;51:684-686. <https://doi.org/10.1111/j.1365-2621.1986.tb13911.x>.
30. Samouillan V, Delaunay F, Dandurand J, et al. The use of thermal techniques for the characterization and selection of natural biomaterials. *J Funct Biomater.* 2011;2:230-248. <https://doi.org/10.3390/jfb2030230>.
31. Sharabi M, Levi-Sasson A, Wolfson R, et al. The mechanical role of the radial fiber network within the annulus fibrosus of the lumbar intervertebral disc: a finite elements study. *J Biomech Eng.* 2018;141:021006. <https://doi.org/10.1115/1.4041769>.
32. Williams JR, Natarajan RN, Andersson GBJ. Inclusion of regional poroelastic material properties better predicts biomechanical behavior of lumbar discs subjected to dynamic loading. *J Biomech.* 2007;40:1981-1987. <https://doi.org/10.1016/j.jbiomech.2006.09.022>.
33. Yang B, O'Connell GD. Effect of collagen fibre orientation on intervertebral disc torsion mechanics. *Biomech Model Mechanobiol.* 2017;16:2005-2015. <https://doi.org/10.1007/s10237-017-0934-2>.
34. Liu X, Krishnamoorthy D, Lin L, et al. A method for characterising human intervertebral disc glycosaminoglycan disaccharides using liquid chromatography-mass spectrometry with multiple reaction monitoring. *Eur Cell Mater.* 2018;35:117-131. <https://doi.org/10.22203/eCM.v035a09>.
35. van den Akker GGH, Koenders MI, van de Loo FAJ, van Lent PLEM, Blaney Davidson E, van der Kraan PM. Transcriptional profiling distinguishes inner and outer annulus fibrosus from nucleus pulposus in the bovine intervertebral disc. *Eur Spine J.* 2017;26:2053-2062. <https://doi.org/10.1007/s00586-017-5150-3>.
36. Bezci SE, Nandy A, O'Connell GD. Effect of hydration on healthy intervertebral disk mechanical stiffness. *J Biomech Eng.* 2015;137:101007. <https://doi.org/10.1115/1.4031416>.
37. Urban JPG, Maroudas A. Swelling of the intervertebral disc in vitro. *Connect Tissue Res.* 1981;9:1-10. <https://doi.org/10.3109/03008208109160234>.
38. Sharma RR, Pollock K, Hubel A, McKenna D. Mesenchymal stem or stromal cells: a review of clinical applications and manufacturing practices. *Transfusion.* 2014;54:1418-1437. <https://doi.org/10.1111/trf.12421>.
39. Nerlich AG, Schaaf R, Wälchli B, Boos N. Temporo-spatial distribution of blood vessels in human lumbar intervertebral discs. *Eur Spine J.* 2007;16:547-555. <https://doi.org/10.1007/s00586-006-0213-x>.
40. Melrose J, Ghosh P, Taylor TKF. Proteoglycan heterogeneity in the normal adult ovine intervertebral disc. *Matrix Biol.* 1994;14:61-75. [https://doi.org/10.1016/0945-053X\(94\)90030-2](https://doi.org/10.1016/0945-053X(94)90030-2).
41. Périé D, Korda D, Iatridis JC. Confined compression experiments on bovine nucleus pulposus and annulus fibrosus: sensitivity of the experiment in the determination of compressive modulus and hydraulic permeability. *J Biomech.* 2005;38:2164-2171. <https://doi.org/10.1016/j.jbiomech.2004.10.002>.
42. Perie DS, MacLean JJ, Owen JP, Iatridis JC. Correlating material properties with tissue composition in enzymatically digested bovine annulus fibrosus and nucleus pulposus tissue. *Ann Biomed Eng.* 2006;34:769-777. <https://doi.org/10.1007/s10439-006-9091-y>.
43. Werbner B, Spack K, O'Connell GD. Bovine annulus fibrosus hydration affects rate-dependent failure mechanics in tension. *J Biomech.* 2019;89:34-39. <https://doi.org/10.1016/j.jbiomech.2019.04.008>.
44. Franklin L, Hull EW. Lipid content of the intervertebral disc. *Clin Chem.* 1966;12:253-257.
45. Bonner WM, Jonsson H, Malanos C, Bryant M. Changes in the lipids of human articular cartilage with age. *Arthritis Rheum.* 1975;18:461-473. <https://doi.org/10.1002/art.1780180505>.
46. Daemen S, van Polanen N, Hesselink MKC. The effect of diet and exercise on lipid droplet dynamics in human muscle tissue. *J Exp Biol.* 2018;221:jeb167015. <https://doi.org/10.1242/jeb.167015>.
47. Finlayson R, Woods SJ. Lipid in the Achilles' tendon. A comparative study. *Atherosclerosis.* 1975;21:371-389. [https://doi.org/10.1016/0021-9150\(75\)90050-7](https://doi.org/10.1016/0021-9150(75)90050-7).
48. Rabinowitz JL, Gregg JR, Nixon JE, Schumacher HR. Lipid composition of the tissues of human knee joints. I. Observations in normal joints (articular cartilage, meniscus, ligaments, synovial fluid, synovium, intra-articular fat pad and bone marrow). *Clin Orthop Relat Res.* 1979;143:260-265.
49. Kannus P, Jozsa L. Histopathological changes preceding spontaneous rupture of a tendon: a controlled study of 891 patients. *J Bone Joint Surg Am.* 1991;73:1507-1525. <https://doi.org/10.2106/00004623-199173100-00009>.
50. Albro MB, Bergholt MS, St-Pierre JP, et al. Raman spectroscopic imaging for quantification of depth-dependent and local heterogeneities in native and engineered cartilage. *npj Regen Med.* 2018;3:3. <https://doi.org/10.1038/s41536-018-0042-7>.
51. Lim NSJ, Hamed Z, Yeow CH, Chan C, Huang Z. Early detection of biomolecular changes in disrupted porcine cartilage using polarized Raman spectroscopy. *J Biomed Opt.* 2011;16:017003. <https://doi.org/10.1117/1.3528006>.
52. Pezzotti G, Boffelli M, Miyamori D, et al. Raman spectroscopy of human skin: looking for a quantitative algorithm to reliably estimate human age. *J Biomed Opt.* 2015;20:065008. <https://doi.org/10.1117/1.jbo.20.6.065008>.
53. Unal M, Yang S, Akkus O. Molecular spectroscopic identification of the water compartments in bone. *Bone.* 2014;67:228-236. <https://doi.org/10.1016/j.bone.2014.07.021>.
54. Wolthuis R, van Aken M, Fountas K, Robinson JS, Bruining HA, Puppels GJ. Determination of water concentration in brain tissue by Raman spectroscopy. *Anal Chem.* 2001;73:3915-3920. <https://doi.org/10.1021/ac0101306>.
55. Bonifacio A, Sergio V. Effects of sample orientation in Raman microspectroscopy of collagen fibers and their impact on the interpretation of the amide III band. *Vib Spectrosc.* 2010;53:314-317. <https://doi.org/10.1016/j.vibspec.2010.04.004>.
56. Flach CR, Moore DJ. Infrared and Raman imaging spectroscopy of ex vivo skin. *Int J Cosmet Sci.* 2013;35:125-135. <https://doi.org/10.1111/ics.12020>.
57. Gniadecka M, Nielsen OF, Wessel S, Heidenheim M, Christensen DH, Wulf HC. Water and protein structure in photoaged and chronically aged skin. *J Invest Dermatol.* 1998b;111:1129-1133. <https://doi.org/10.1046/j.1523-1747.1998.00430.x>.
58. Talari ACS, Movasaghi Z, Rehman S, Rehman IU. Raman spectroscopy of biological tissues. *Appl Spectrosc Rev.* 2015;50:46-111. <https://doi.org/10.1080/05704928.2014.923902>.
59. Manoharan R, Wang Y, Feld MS. Histochemical analysis of biological tissues using Raman spectroscopy. *Spectrochim Acta A Mol Biomol Spectrosc.* 2003;52:215-249. [https://doi.org/10.1016/0584-8539\(95\)01573-6](https://doi.org/10.1016/0584-8539(95)01573-6).
60. Téllez Soto CA, Medeiros-Neto LP, dos Santos L, et al. Infrared and confocal Raman spectroscopy to differentiate changes in the protein secondary structure in normal and abnormal thyroid tissues. *J Raman Spectrosc.* 2018;49:1165-1173. <https://doi.org/10.1002/jrs.5370>.
61. Brooks J. Bound water in muscle. *J Gen Physiol.* 1934;17:783-790. <https://doi.org/10.1085/jgp.17.6.783>.
62. Tang R, Samouillan V, Dandurand J, et al. Thermal and vibrational characterization of human skin. *J Therm Anal Calorim.* 2017;127:1143-1154. <https://doi.org/10.1007/s10973-016-5384-z>.
63. Zhang Q, Andrew Chan KL, Zhang G, et al. Raman microspectroscopic and dynamic vapor sorption characterization of hydration in collagen and dermal tissue. *Biopolymers.* 2011;95:607-615. <https://doi.org/10.1002/bip.21618>.

64. Agee KA, Prakki A, Abu-Haimed T, et al. Water distribution in dentin matrices: bound vs. unbound water. *Dent Mater.* 2015;31:205-216. <https://doi.org/10.1016/j.dental.2014.12.007>.
65. Cortes DH, Jacobs NT, DeLucca JF, Elliott DM. Elastic, permeability and swelling properties of human intervertebral disc tissues: a benchmark for tissue engineering. *J Biomech.* 2014;47:2088-2094. <https://doi.org/10.1016/j.jbiomech.2013.12.021>.
66. Padalkar MV, Spencer RG, Pleshko N. Near infrared spectroscopic evaluation of water in hyaline cartilage. *Ann Biomed Eng.* 2013;41:2426-2436. <https://doi.org/10.1007/s10439-013-0844-0>.
67. Aktaş N, Tülek Y, Gökalp HY. Determination of differences in free and bound water contents of beef muscle by DSC under various freezing conditions. *J Thermal Anal.* 1997;50:617-624. <https://doi.org/10.1007/bf01979033>.
68. Huang Z, Delparastan P, Burch P, Cheng J, Cao Y, Messersmith PB. Injectable dynamic covalent hydrogels of boronic acid polymers cross-linked by bioactive plant-derived polyphenols. *Biomater Sci.* 2019;6:2487-2495. <https://doi.org/10.1039/C8BM00453F>.
69. Miles CA, Ghelashvili M. Polymer-in-a-box mechanism for the thermal stabilization of collagen molecules in fibers. *Biophys J.* 1999;76:3243-3252. [https://doi.org/10.1016/S0006-3495\(99\)77476-X](https://doi.org/10.1016/S0006-3495(99)77476-X).
70. Bozec L, Odlyha M. Thermal denaturation studies of collagen by microthermal analysis and atomic force microscopy. *Biophys J.* 2011;101:228-236. <https://doi.org/10.1016/j.bpj.2011.04.033>.
71. Chae Y, Protsenko D, Lavernia EJ, Wong BJF. Effect of water content on enthalpic relaxations in porcine septal cartilage. *J Therm Anal Calorim.* 2009;95:937-943. <https://doi.org/10.1007/s10973-007-8782-4>.
72. Ghosh P, Bushell GR, Taylor TFK, Akeson WH. Collagens, elastin and non-collagenous protein of the intervertebral disk. *Clin Orthop Relat Res.* 1977;129:124-132. <https://doi.org/10.1097/00003086-197711000-00014>.
73. Ranjit S, Dvornikov A, Stakic M, et al. Imaging fibrosis and separating collagens using second harmonic generation and Phasor approach to fluorescence lifetime imaging. *Sci Rep.* 2015;5:13378. <https://doi.org/10.1038/srep13378>.
74. Kudo K, Ishida J, Syuu G, Sekine Y, Ikeda-Fukazawa T. Structural changes of water in poly(vinyl alcohol) hydrogel during dehydration. *J Chem Phys.* 2014;140:044909. <https://doi.org/10.1063/1.4862996>.

SUPPORTING INFORMATION

Additional supporting information may be found online in the Supporting Information section at the end of this article.

How to cite this article: Bezci SE, Werbner B, Zhou M, et al. Radial variation in biochemical composition of the bovine caudal intervertebral disc. *JOR Spine.* 2019;2:e1065. <https://doi.org/10.1002/jsp2.1065>